Predicted Effects of Confinement on the Melting Transition in Krypton-Argon Adlayers

K. Bader and M.W. Roth
Physics Department
University of Northern Iowa
Cedar Falls, Iowa 50614-0150 USA

Received February 4, 2002 Accepted March 7, 2002

ABSTRACT

We report the results of (N,ρ,T) Molecular-Dynamics computer simulations of krypton-argon mixtures physisorbed between two graphite sheets. Three novel aspects of the system's behavior emerge from this study. To begin with, new high-temperature commensurate solid phases for both argon and krypton as a result of confinement are predicted, as well as a family of confinement-induced solid-liquid phase transitions. In addition, we observe that the melting temperature of the system can be adjusted within a given range by the graphite sheet spacing. Finally, in the case of argon-krypton mixtures, certain temperatures and sheet spacings result in almost complete impurity extraction.

I. INTRODUCTION

For decades now researchers have studied the behavior of atomic and molecular species physisorbed onto graphite. For rare gas adsorbates such as krypton and argon the phase diagrams have been mapped out rather thoroughly on both experimental and computational fronts. Although the discovery of fullerenes and nanotubes has spurred scientific interest into adsorption of rare gasses onto new geometries, comparatively little has been done to study the phase transitions of physisorbed systems in confined geometries [1-4].

Both the nature and temperature of melting for commensurate monolayers on graphite (including krypton) are highly sensitive to density fluctuations at completion (an area density of 0.0636 atom/Å^2 for a monolayer) and density fluctuations in this regime are in turn strongly coupled to the vertical (out-of-plane, or $\hat{z}$) excursions of the adsorbed species. It follows, then, that the vertical boundary conditions for the system play an important role in melting. The purpose of this study is to simulate the effects of altering the $\hat{z}$ boundary conditions on physisorbed rare gas layers by modeling adsorption of the krypton-argon mixtures between two graphite sheets. The species are chosen as such because both krypton [5-20] and argon [21-33] have been studied as single layers on graphite extensively and they exhibit markedly different adsorption behavior, thus having a high potential to show the effects of selectivity imposed by the presence of the second sheet. New high-temperature commensurate solids and new confinement-induced solid-liquid phase transitions for both krypton and argon emerge from this study. As will be discussed later, this is a result of the adlayer's being forced into a region where atoms' lateral interaction with the graphite surface is very strong. Secondly, and not entirely surprisingly, we find that the melting transition in both nature and temperature can be fine-tuned purely by the spacing of the graphite sheets. Moreover we are able to explain the dependence of the melting transition on sheet spacing simply as an outcome of competition between confinement and attraction with the upper graphite sheet. Lastly, we present the results for a 50% argon-krypton mixed adlayer and observe that for certain graphite spacings and temperatures, the upper sheet adsorbs almost pure argon, suggesting that with some experimental refinement, impurity extraction can be attained.

Figure 1. The Cartesian coordinate system used in this study (standard). The x-axis lies along the Γ-K direction of the graphite lattice and the y-axis is along the Γ-M direction. The z-axis is perpendicular to the substrate plane. There are an infinite number of graphite planes considered but we show only three.

II. ABOUT THE SIMULATIONS

A constant-density, constant-temperature molecular-dynamics method is utilized in this study. There are a total of 400 atoms in the computational cell with varying mixture fractions of argon and krypton; they interact at a separation r_{ij} through a Lennard-Jones pair potential

$$u_{LJ}(r_{ij}) = 4\varepsilon_{ij}\left[\left(\frac{\sigma_{ij}}{r_{ij}}\right)^{12} - \left(\frac{\sigma_{ij}}{r_{ij}}\right)^{6}\right]$$

and the mixed interactions (type of atom i ≠ type of atom j) are given by Lorentz-Bertholot combining rules

$$\sigma_{ij} = \frac{\sigma_i + \sigma_j}{2}$$

$$\varepsilon_{ij} = \sqrt{\varepsilon_i\ \varepsilon_j}$$

values for the potential parameters used in our work are shown in Table 1.

The Lennard-Jones potential is chosen because it is widely used in atomic and molecular simulations, including recent work on systems confined in planar geometries [1-4]. This allows better comparisons with other deterministic and stochastic simulation results. Especially in our simulations of close confinement, however, it would be of use to compare the results presented here with an anisotropic Lennard-Jones pair potential which better

	ε (K)	σ (Å)
Argon	**171.0**	**3.60**
Krypton	**120.0**	**3.38**
Mixed	**143.25**	**3.49**

Table 1. Lennard-Jones potential parameters for the adsorbate atoms.

represents the contributions of the graphite p-orbitals. The adsorbate-graphite potential inter-actions $u_i^{Kr\text{-}gr}$ of adsorbate atom (i) located at (x_i,y_i,z_i) in a commonly defined Cartesian coordinate system are of the form proposed by Steele [34],

$$u_i^{gr} = E_{0i}(z_i) + \sum_{n=1}^{\infty} E_{ni}(z_i)\, f_n(x_i, y_i). \qquad (1)$$

This standard coordinate system is re-presented in Figure 1.

The E_{ni} are strong laterally averaged terms and the $f_n(x_i,y_i)$ are periodic functions representing the lateral variation in the interaction energy due to the graphite structure. Only the n=1 term is retained in equation (1) because the series converges very quickly, and the analytical expressions for terms contained in it are

$$E_{0i}(z_i) = \frac{2\pi q \varepsilon \sigma^6}{a_s}\left(\frac{2\sigma^6}{45d(z_i+0.72d)^9} + \frac{2\sigma^6}{5z_i^{10}} - \frac{1}{z_i^4} - \frac{2z_i^2+7z_i d+7d^2}{6d(z_i+d)^5}\right),$$

$$E_{ni}(z_i) = \frac{2\pi\varepsilon\sigma^6}{a_s}\{(\frac{\sigma^6}{30})(\frac{g_n}{2z_i})^5 K_5(g_n z_i) - 2(\frac{g_n}{2z_i})^2 K_2(g_n z_i)\},$$

and

$$f_1(x_i, y_i) = f_n(x_i, y_i)|_{n=1} =$$
$$-2\{\cos\frac{2\pi}{a}(x+(\frac{y}{\sqrt{3}})) + \cos\frac{2\pi}{a}(x-(\frac{y}{\sqrt{3}})) + \cos\frac{4\pi}{a}(\frac{y}{\sqrt{3}})\}.$$

The K_i are modified Bessel functions of the second kind and of order i and the g_n are the magnitudes of the n^{th} graphite reciprocal lattice vectors; other important parameters appearing in the expressions for the potential are identified in Table 2.

In Steele's original Fourier expansion the basal plane of the graphite sheet is at z=0 and an infinite number of graphite layers extends in the $-\hat{z}$ direction. In the work presented here the surface of the basal plane extends in either the $+\hat{z}$ or the $-\hat{z}$ direction, depending upon where the sheet is placed. One graphite sheet has a face at z=0 and extends in the $-\hat{z}$ direction; the other is inverted and its face is at z=h, where h ranges anywhere from 5 Å to 11 Å.

Periodic boundary conditions are implemented in the (x,y) plane. Initially, the atoms are placed at as though they were adsorbed to the bottom graphite sheet in a triangular commensurate lattice. When more than one species is present, atom types are assigned in a random sequence so as to avoid impurity patches in favor of an annealed sample.

Parameter	Symbol	Value
Ar-graphite potential Parameters	**ε,σ**	**54.46K, 3.11Å**
Kr-graphite potential parameters	**ε,σ**	**64.83K, 3.22Å**
Graphite plane spacing	**d**	**3.37 Å**
Area of graphite unit cell	**a_s**	**5.24 Å^2**
Atom number in graphite unit cell	**q**	**2**

Table 2. Relevant parameters for the ad-atom-graphite interactions.

The system is allowed to equilibrate for anywhere from 50,000 to 100,000 time steps (ranging anywhere from 0.001 picoseconds to 0.003 picoseconds) and subsequently the production runs (over which meaningful thermal averages are calculated) range over the next 10,000 to 20,000 time steps. The thermostat involves uniform velocity rescaling and a standard Verlet algorithm is used to integrate the equations of motion.

The size of the computational cell was chosen so that we could have the largest number of atoms in the simulation (in order to capture the important physics of the system) and still completes the project in a reasonable time. In addition we chose to use constant-density and constant-temperature Molecular Dynamics because we wanted to simulate experimental systems as closely as possible, and such conditions are reasonable representations of adsorbates on single graphite sheets, which we interpret to be extendable to planar geometries in general. In addition, Molecular Dynamics allows us to track a dynamical (time) sequence for the system, which stochastic methods are much less efficient at.

III. THE HIGH-TEMPERATURE SOLIDS

Figure 2 shows the order parameter O1 for pure krypton as functions of graphite sheet spacing h at various temperatures, as well as one curve for pure argon at T = 20 K. The expression for O1 is

$$O1 = \frac{1}{6N}\sum_{i=1}^{N}\left\langle \sum_{s=1}^{6} e^{i\vec{g}_s \bullet \vec{r}_i} \right\rangle$$

Here the sum is over the six reciprocal lattice vectors g_s for the graphite substrate, r_i locates adsorbate atom (i) and brackets (<…>) denote a time, or thermal average. O1 is useful because it is an indicator of the degree of translational order of the adsorbate; O1 is equal to unity for a static, registered lattice and it vanishes for either an infinite incommensurate lattice, or in the fluid where the atoms evenly sample positions over the graphite plane with uniform probability density in space.

Since the first term in equation (1) is strong and laterally averaged, its only spatial

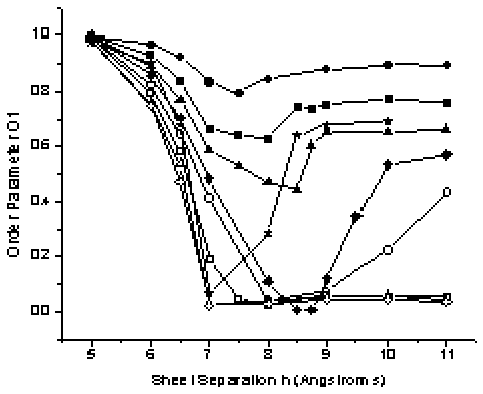

Figure 2. Order parameter O1 as functions of graphite sheet spacing h for T = 20 K (solid circles), T = 40 K (solid squares), T = 60 K (solid triangles), T = 80 K (solid diamonds), T = 100 K (hollow circles), T = 120 K (hollow squares), T = 140 K (hollow triangles) and T = 160 K (hollow diamonds). Also, O1 for argon is shown at T = 20 K with stars.

dependence is vertical. Its thermal average per particle is

$$< E_0 > = \frac{1}{N}\sum_{i=1}^{N} < E_{0i} > \qquad (2)$$

where N is the number of atoms in the simulation. When calculated individually for adsorbate atom interactions with each sheet, $<E_0>$ is a good measure of the vertical behavior of the adlayer and can provide some perspective on the degree of vertical fluctuations of the adsorbate as well as sheet-to-sheet atomic migration. The n = 1 term under the sum in equation (1) describes the periodicity in the energy due to the substrate corrugation and is roughly two orders of magnitude smaller than $E_0(z_i)$ for conventional monolayers. Because $f_1(x_i,y_i)$ is a periodic function which has its minima at the graphite hexagon centers, its thermal average $<E_1f_1>$ (referred to as $<E_1>$ and calculated in a manner similar to the thermal average in equation (2)) calculated for interactions with each sheet separately are reliable indicator of registry (the degree to which atoms tend to sample areas over graphite hexagon centers) as well as melting. Figure 3 shows the thermal

averages $\langle E_0 \rangle$ per particle for interactions with the bottom sheet only as functions of graphite sheet spacing. Figure 4 shows $\langle E_1 \rangle$ per particle for interactions with the bottom sheet only as functions of graphite sheet spacing for various temperatures.

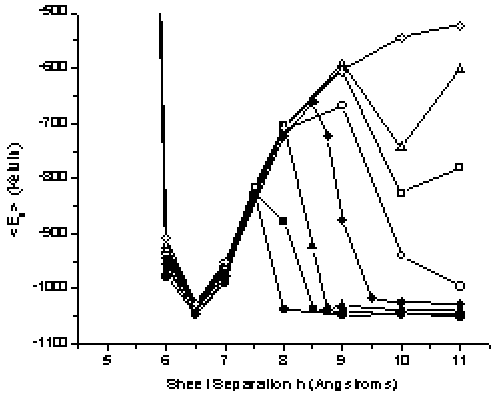

Figure 3. $\langle E_0 \rangle$ as functions of graphite sheet spacing h for interactions with the bottom sheet only and at various temperatures. The legend is the same as in Figure 2 except that no curves are offset. To aid resolution, values for h below 6 Å are not shown.

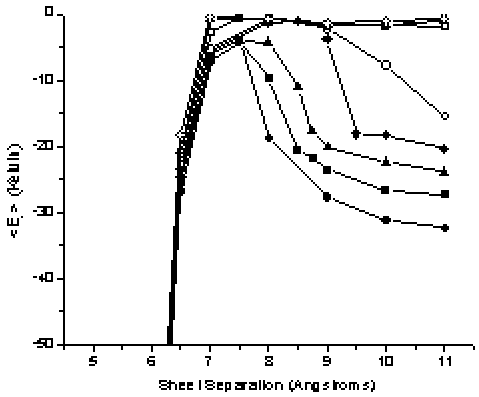

Figure 4. $\langle E_1 \rangle$ as functions of graphite sheet spacing for interactions with the bottom sheet only and at various temperatures. The format is the same as in Figure 3. To aid resolution, values for h below 6 Å are not shown.

The behavior of O1 shows that at sufficiently low temperatures (less than about 60K) the system will not exist as a fluid, although the minima in the curves illustrate that at a given separation (which increases with temperature due to vertical thermal expansion) the second sheet is able to augment vertical fluctuations, thus leaving more in-plane room for the adsorbate thus decreasing spatial order. This is confirmed by the fact that the points of minimum O1 are points of local maxima in $\langle E_0 \rangle$ and $\langle E_1 \rangle$. For temperatures greater that 80K, O1 shows that varying the sheet separation can cause the system to undergo a series of solid-fluid phase transitions. Moreover, inspection of figures 3 and 4 illustrates as the sheet separation is decreased from the point of minimum O1, the laterally averaged energy term $\langle E_0 \rangle$ rises but $\langle E_1 \rangle$ sharply decreases. The strong mutual vertical repulsion between the graphite planes forces the atoms into very deep lateral potential wells so this effect increases the undulation in the potential due to the graphite structure, thus confining the system in the (x,y) plane. The deep lateral wells are not sampled by atoms adsorbed onto a single sheet of graphite because the much stronger laterally averaged term $E_0(z_i)$ keeps them too far above the graphite surface to do so. However with two graphite sheets present it is possible to force the atoms into this interesting and new regime and $E_1(z_i)$, the vertically dependent multiplier of $f_1(x_i,y_i)$, becomes very large thus magnifying the lateral corrugation in the graphite. Although we are not able to detect solid-solid phase transitions for krypton below 60 K, it is clear that at the highest temperatures shown (T = 140 K and T = 160 K) our simulations predict a new confined high-temperature commensurate solid phase because the system exists as a liquid for O1 $\leq$ 0.25. At low temperature (T = 20 K), O1 for argon also shows that, as sheet separation is decreased there are two transitions; one from the incommensurate solid to the fluid and then from the fluid to the high-temperature commensurate confined solid. The completion of the series of O1 for pure argon at higher temperatures, required to map out more solid-liquid transitions as well as the effects of confinement on the fluid, is in progress.

IV. THE DEPENDENCE OF MELTING ON SHEET SEPARATION

Figure 5 shows O1 as functions of temperature and figure 6 shows $<E_0>$ as functions of temperature; both figures are for various sheet spacings for pure krypton layers. Figure 7 shows the melting temperature T_m as a function of sheet spacing also for pure krypton layers.

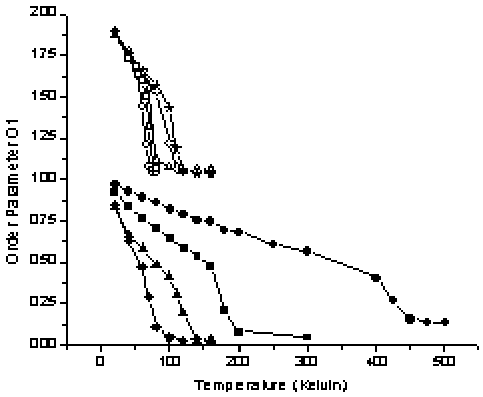

Figure 5. Order parameter O1 as functions of temperature T for graphite sheet spacings of 6 Å(solid squares), 6.5 Å (solid triangles), 7 Å (solid diamonds), 8 Å (hollow circles), 9 Å (hollow squares),10 Å (hollow triangles) and 11 Å (hollow diamonds). Values for h = 5 Å are not shown, as melting is not observed for that separation. For visual ease the curves for h ≥ 8 Å are offset by one unit.

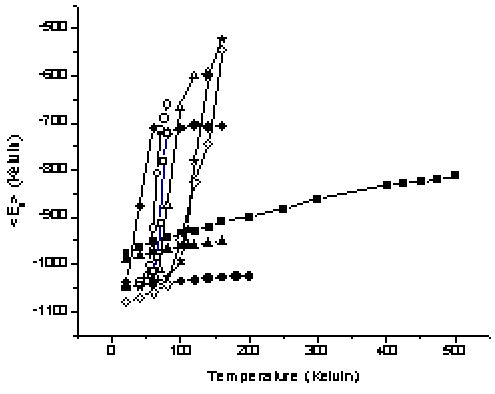

Figure 6. $<E_0>$ as functions of temperature T for interactions with the bottom sheet only and at various graphite sheet spacings. The format is the same as in Figure 5 except that no curves are offset.

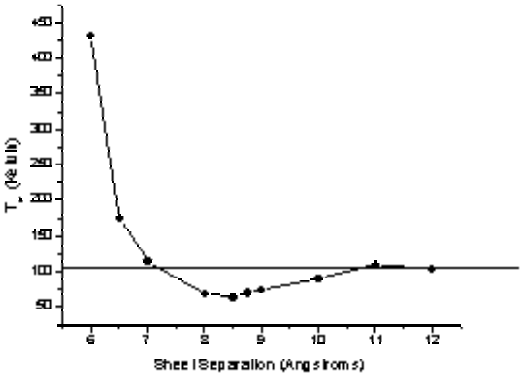

Figure 7. Melting temperature T_m as a function of graphite sheet spacing h. The horizontal line represents the melting temperature for the infinite-separation calculation.

The minimum in T_m (T) at about T_m = 70 K suggests that two competing effects are influencing the melting transition. Inspection of $<E_0>$ reveals that at sheet spacings below 8 Å there is no sharp rise as temperature is increased, but for spacings greater than 8 Å there are. This confirms that, in addition to the large lateral corrugation of the surface experienced as the atoms come closer to the graphite, confinement (dominant at sheet spacings below the minimum) is raising the melting temperature by stifling vertical fluctuations thus reducing in-plane room for the adsorbate. Also, it shows that attraction of the atoms to the upper sheet (dominant at sheet separations above the minimum) enhance vertical atomic fluctuations and effectively lowers the area density of the layer adsorbed on to the bottom sheet. At sheet separations greater that 8 Å , which are near the minimum in T_m, the upper sheet prompts melting, as atoms are adsorbed onto the upper sheet at a temperature lower than melting , thus reducing planar density of the bottom layer. Since the attraction of the adsorbate to the upper sheet becomes less prominent as graphite separation is increased, the enhancement of vertical excursions weakens as the sheet spacing is increased from its value at the minimum melting temperature and the melting temperature closely approaches (single plane experimental) value of T_m = 129K asymptotically [5-20]. Figures 5 and 6 also

show an observation consistent with asymptotic behavior: namely that, as sheet separation increases, the large vertical jumps in $<E_0>$ occur at higher temperatures. In fact, for sheet separations greater than 9 Å, melting occurs before vertical excursions do, which is a signature of the familiar single sheet melting transition occurring before desorption. O1 clearly shows that the effects of confinement become important at low temperature, as the curves become more and more separated in the solid with sheet separations decreasing from about 7 Å. On the contrary, for sheet separations greater than that, O1 in the solid coincide. The sharpness of melting remains similar for sheet separations greater than 6 Å, but clearly it becomes less sharp as the effects of confinement become more pronounced.

It is interesting to note that, for $<E_0>$ in figure 3 there seems to be oscillatory behavior for T = 120 K and 140 K between 9 Å and 11 Å. This feature is not seen in any other quantity and is purely related to the vertical behavior of the system; the lower values of $<E_0>$ occur at points where the graphite plane separation stabilizes multilayer promotion, i.e. where second layer promotion and adsorption onto either graphite sheet are both occurring as they would in the single-sheet case. That is, the configuration of the two-sheet system is stabilized when it resonates with that of the one sheet monolayer or multilayer system. This oscillatory behavior is reminiscent of that in the solvation force [1-4], density [1-4] and adsorption excess [2] observed in previous simulations other planar-confined systems.

V. IMPURITY EXTRACTION

We also performed simulations with various mixtures of krypton and argon. Initially all the atoms are adsorbed to the bottom plane. For both species, a gradual increase in adsorption onto the top sheet is followed by a sharp increase near melting, after which both sheets share species equally. However it is interesting to note that there is a temperature region for both plane separations (lower temperatures for the closer sheets) shown where the top sheet adsorbate is almost pure argon. This suggests that, with some refinement, two-sheet adsorption could serve as a method of impurity extraction for adsorbate mixtures of sufficiently different proprieties, such as in this study. Figure 8(a-c) shows ray-traced renderings for a 50% argon - krypton mixture adsorbed onto two graphite sheets separated by 11 Å, providing a visual illustration of low-temperature bottom layer adsorption (T = 40 K), almost pure argon adsorbing to the top layer before melting (T = 80 K), and the high-temperature (T = 140 K) equal sharing of the components between layers.

VI. FINAL REMARKS

It appears that in general adsorption of adlayers onto multiple graphite sheets can provide very interesting and useful results, and possibly lend insight into similar 3D experimental work [35]. In a future study we plan to address the changes in system behavior that are brought about by changing argon-krypton mixture fractions. Since it seems possible to fine-tune the melting transition within a certain range, investigation of any properties of the system that change across melting could lead to very useful applications. We wish to emphasize that the limits of the physical viability of our results reside primarily in the potential interactions we use. The potentials used are clearly appropriate for conventional monolayers. As the graphite sheets are brought close together, it could be that either the p orbitals could affect the confinement in an unforeseen way, or that the graphite-graphite interaction could alter the electronic structure on the substrate surface in a way unforeseen by this study.

ACKNOWLEDGEMENTS

This work has been supported by a University of Northern Iowa four-week summer fellowship. Both authors thank the University of Northern Iowa for the use of the Physics Department computing facilities. The second author (MWR) gratefully acknowledges helpful and encouraging discussions with Bill Steele at the Penn State University Department of Chemistry. In addition both authors are grateful to the referees for helpful comments.

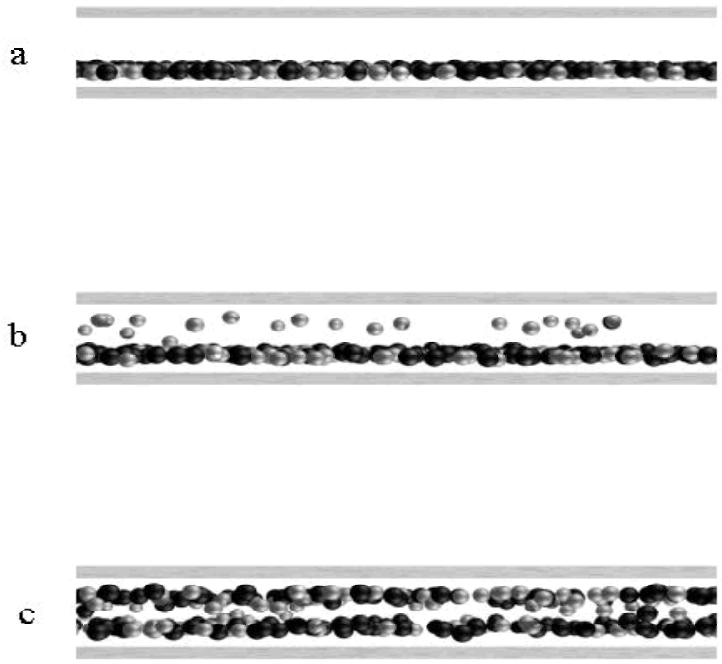

Figure 8 (a-c). Ray-traced renderings of the 50% argon-krypton mixture for a sheet separation of 11Å at T = 40 K (top), T = 80 K (middle) and T = 140 K (bottom), respectively. The lighter shaded atoms are argon and the gray plans represent the surfaces of the graphite sheets; all sizes are to scale.

REFERENCES

1. Philippe Bordarier, Bernard Rousseau and Alain H. Fuchs, *Mol. Sym. 17*, 199 (1996), and references therein.
2. I.K. Snook and W. van Megen, *J. Chem. Phys. 72*, 907 (1980).
3. Mark Lupkowski and Frank van Swol, *J. Chem. Phys. 93,*737 (1990).
4. Laura J. Frink and Frank van Swol, *J. Chem. Phys. 100*, 106 (1994).
5. N.D. Shrimpton, M. W. Cole and W. A. Steele (private communication).
6. E.D. Specht et al., *Zeit. Phys. B 69*, 347 (1987).
7. D.M. Butler, J. A. Litzinger and G. A. Stewart, *Phys. Rev. Lett. 44*, 466 (1980).
8. J. Birgenau et al., *Ordering in Two Dimensions*, Elsevier North Holland Publishing *29* (1980).
9. S.Chung et al., *Phys. Rev. B 35*, 4870 (1987).
10. M.D. Chinn and S. C. Fain, Jr., *Phys. Rev. Lett. 39*, 146 (1977).
11. C.A. Guryanet al., *Phys. Rev. B 37*, 3461 (1988).
12. R. Hoja and R. Marx, *Phys. Rev. B 34*, 7823 (1986).
13. A. Inaba, J. A. Morrison and J. M Telfer, *Mol. Phys. 162*, 961 (1987).

14. N. Dupont-Pavlovsky, C. Bockel and A. Thomy, *Surf. Sci. 160*, 12 (1985).
15. Y. Larher and A. Terlain, *J. Chem. Phys. 72*, 1052 (1980).
16. T.P. Vo and T. Fort, Jr., *J. Phys. Chem. 91*, 6638 (1987).
17. J.A. Venables et al., *Surf. Sci. 145*, 345 (1984).
18. T.H. Ellis et al., *Surf. Sci. 155*, 499 (1985).
19. R. M. Suter and N. J. Colella, R. Gangwar, *Phys. Rev. B 31*, 627 (1985).
20. K.J. Niskanen and R. B. Griffiths, *Phys. Rev. B 32*, 5858 (1985).
21. Thomas T. Chung, *Surf. Sci*. *87*, 348 (1979).
22. A. D. Migone, Z. R. Li and M.H.W. Chan, *Phys. Rev. Lett. 53*, 810 (1984).
23. Y. Lahrer, *Surf. Sci. 134*, 469 (1983).
24. Q.M Zhang and J.Z. Larese, *Phys. Rev. B 43*, 938 (1991).
25. M. D. Chinn and S. C. Fain, Jr., *Phys. Rev. Lett. 39*, 146 (1977).
26. H. Taub et al., *Phys. Rev. B 16*, 4551 (1977).
27. M. Nielsen et al., *Phys.Rev. B 35*, 1419 (1987).
28. Christopher G. Shawet al., *Phys. Rev. Lett. 41*, 955 (1978).
29. K.L. D'Amico et al., *Phys. Rev. B 41*, 4638 (1990).
30. C.R. Fuselier, J.C. Raich and N.S. Gillis, *Surf. Sci. 92*, 667 (1980).
31. F. F. Abraham, *Phys. Rev. B 28*, 7338 (1983).
32. F.E. Hanson, M.J. Mandell and J.P. McTague, *J. Physique* **38**, C4-76 (1977).
33. James M. Phillips, *Phys. Lett. A* **147**, 54 (1990).
34. W.A. Steele, *Surf. Sci.* **36**, 317 (1973).
35. D.W. Brown, P.E.Sokol and S.N. Ehrlich, *Phys. Rev. Lett.* **81**, 1019 (1998).